The International Journal of Advanced Manufacturing Technology (2018) 98:2213–2230
https://doi.org/10.1007/s00170-018-2374-2

ORIGINAL ARTICLE

Experimental investigation and multi-objective optimization of Nd:YAG laser micro-channeling process of zirconia dental ceramic

Basem M. A. Abdo[1,2] · Abdulaziz M. El-Tamimi[1] · Saqib Anwar[1] · Usama Umer[2] · Abdulrahman M. Alahmari[1,2] · Mageed A. Ghaleb[1]

Received: 22 March 2018 / Accepted: 25 June 2018 / Published online: 3 July 2018

Abstract

In biomedical applications, micro-channels are one of the important features and are often fabricated by laser ablation process. However, laser-processed micro-channels exhibit crucial issues of heat-affected zone (HAZ), dimensional errors, and poor surface quality. This paper investigates the influence of key laser process parameters on the dimensional accuracy and the surface quality of the micro-channels fabricated on zirconia dental material. A full factorial based on design of experiment (DOE) methodology was adopted for carrying out experiments in a pulsed Nd:YAG laser micro-milling. The process parameters considered during machining were laser scanning speed, pulse frequency, and pulse intensity with four levels for each parameters resulting into 64 individual experiments. Channel dimensional accuracy (depth error, top width error and taper angle), surface roughness (R_a), and HAZ were considered as the performance criteria for the present study. The experimental results show that the scanning speed and the pulse intensity and their interaction have the most influential effects on the depth error and HAZ. Moreover, it was found that the pulse intensity controls R_a, and the top width error is mainly affected by the scanning speed. The pulse frequency has the main effect on the channel taper angle, while its effects on other responses are negligible. The multi-objective genetic algorithm (MOGA-II) was employed to determine the optimal parametric conditions for minimizing the ablated depth errors and HAZ while putting the constraints on the minimum acceptable levels of the surface roughness, top width error, and taper angle. The optimized solutions were obtained at the moderate levels of scanning speed and pulse intensities and low levels of pulse frequencies.

Keywords Nd:YAG laser · Zirconia dental · Micro-channel · Optimization · HAZ · Ceramic

✉ Basem M. A. Abdo
babdo@ksu.edu.sa

Abdulaziz M. El-Tamimi
atamimi@ksu.edu.sa

Saqib Anwar
sanwar@ksu.edu.sa

Usama Umer
usamaumer@yahoo.com

Abdulrahman M. Alahmari
alahmari@ksu.edu.sa

Mageed A. Ghaleb
mghaleb87@gmail.com

[1] Industrial Engineering Department, College of Engineering, King Saud University, Riyadh 12372, Saudi Arabia

[2] Princess Fatima Alnijiris's Research Chair for Advanced Manufacturing Technology (FARCAMT Chair), Advanced Manufacturing Institute, King Saud University, Riyadh, Saudi Arabia

Abbreviations

Adj MS	Adjusted mean squares
Adj SS	Adjusted sum of squares
ANOVA	Analysis of variance
DE	Depth error
DOE	Design of experiments
F	Pulse frequency
HAZ	Heat affected zone
I	Pulse intensity
LBMMP	Laser beam micro-machining process
MOGA	Multi-objective genetic algorithm
MRR	Material removal rate
Nd:YAG	Neodymium-doped yttrium aluminum garnet
Ra	Arithmetic mean surface roughness
RSM	Response surface methodology
SEM	Scanning electron microscope
TWE	Top width error
V	Scanning speed

1 Introduction

Nowadays, there is a continuously growing interest in the process of micro-machining in developing of micro-features, for example, micro-channels and micro-holes in various advanced ceramic materials such as alumina and zirconia. This is due to the increasing demand for highly accurate miniaturized and lightweight components for various applications such as medical, aerospace, MEMS, and automotive. Among several machined micro-features, the micro-channels are the typical features that have several applications in microfluidic and micro-technology systems and form the basis of the new biomedical devices. Zirconia dental material is very popular in medical ceramics that has superior properties such as high hardness, high strength at elevated temperatures, low density, and high resistance to creep and wear, and chemical degradation. Owing to its excellent properties, zirconia dental has acquired great importance in several medical applications such as micro-fluidics, lab-on-chip, and a dental restoration that relies on precision-machined micro-features [1, 2]. Despite its remarkable properties, zirconia dental material is considered as a difficult-to-cut material by conventional machining processes such as turning, milling, and grinding due to high brittleness and low fracture toughness. Moreover, properties of resistance to chemical degradation and poor electrical conductivity act as an impediment in machining of zirconia materials via chemical machining and electric discharge machining processes [3]. Ultrasonic machining was considered as an alternative process for machining zirconia materials, but it has its limitations such as high machining cost and low material removal rate (MRR) [4–6].

Laser beam micro-machining process (LBMMP) provides a new method of producing micro-features in a variety of materials (including zirconia) regardless of their hardness, thermal, and electrical properties. LBMMP is a thermal non-contact, fast, easy to control, and flexible process. It has rapidly become inexpensive and can machine complex shapes without the need of costly tooling [7–9]. Moreover, LBMMP has the capability of producing micro-features (such as micro-channels and micro-holes) on bio-ceramic materials that have large applications in medical field such as microfluidic, lab on a chip, and microbiology [9, 10]. Despite numerous advantages, laser machining has some drawbacks such as poor surface finish and accuracy, and heat-affected zone (HAZ) is produced. Research must be conducted to overcome these limitations of the laser machining to increase its employability for micro-machining applications; for instance, the HAZ adversely affects the bonding process in microfluidic devices [11]. Several studies have been reported to study the effects of laser micro-machining (including micro-milling, micro-drilling, and micro-turning) process parameters on the quality of the resultant surfaces or geometrical micro-features ablated on various ceramics materials. For example,

Table 1 Summary of various optimization techniques employed in previous studies while laser ablating of advanced ceramics and some other materials

Optimization method	Laser process	Machined feature	Input parameters	Output responses	Substrate	Ref.
Gray relational and RSM	Nd:YAG	Micro-turning	Laser average power, pulse frequency, and feed rate	Surface roughness and machined depth deviation	Alumina	[21, 22]
MOGA-II		Pockets	Pulse duration, pulse frequency, pulse overlaps, and laser intensity	Surface roughness and material removal rate		[23]
Grey relational		Micro-holes	Lamp current, pulse frequency, air pressure, and pulse width	Hole taper and heat-affected zone	Aluminaand zirconia	[24, 25]
RSM		Micro-grooves	Lamp current, pulse frequency, pulse width, assist air pressure, and cutting speed	Deviations of taper and depth	Aluminum titanate Al_2TiO_5	[26]
Multiple objective particle swarm optimization		Micro-channels	Scanning speed, pulse frequency, and pulse intensity	Channel depth, width, surface roughness	AISI H13 tool steel	[27]
Taguchi and Grey relational			Scanning speed, pulse frequency, and pulse width	Depth, burr height, and burr width	PMMA	[28]
RSM	Nd:YVO4		Scanning speed, pulse frequency, and laser intensity	Channel dimensions (top width, bottom width, depth, taperness)	Inconel 718	[29]
		Micro-pockets	Scanning speed, laser power, q-switch frequency, loop number, and duty cycle	Surface quality, pocket depth	Titanium sheets	[30]

Table 2 Chemical composition and mechanical, optical, and thermal properties of zirconia dental material used for experimentation

Property	Value
$ZrO_2 + HfO_2 + Y_2O_3$ (%)	≥ 99.0
Y_2O_3 (%)	4.5–5.6
HfO_2 (%)	1.8–2.2
Al_2O_3 (%)	0.03–0.07
Other oxides (%)	≤ 0.5
Flexural strength (MPa)	1200
Vickers hardness (HV 0.5)	1250
Young's modulus (GPa)	210
Density (g/cm^3)	≥ 6.07
Fracture toughness, K_{IC} (MPa m^{-1})	12
Refractive index for 3 mol% Y-TZP	2.214
Birefringence, for 3 mol% Y-TZP	0.038
Thermal expansion coefficient,WAK 20–600 °C (10–6 K^{-1})	10.7
melting point (°C)	2700

fabrication of micro-channels and micro-pits on ceramic (Al_2O_3) surface was reported in [12], wherein Nd:YAG-laser was applied to reduce the coefficient of friction of the machined substrates. In the study documented in [13], femtosecond pulsed laser was applied for drilling blind and through holes in titanium carbide ceramic. The results revealed that laser intensity and the repetition rate have more effect on the material removal rate and the quality of the machined micro-holes. Chen et al. [14] developed a prediction model to investigate the effects of material properties and laser parameters on the ablation depth and squared crater diameter per pulse of micro-holes drilled on Al_2O_3 ceramics. The authors in [15] used nanosecond laser to fabricate precise micro-feature on yttria-tetragonal zirconia polycrystal ceramic. Different laser parameters were investigated to achieve high-quality micro-sized step (500 μm width, 100 μm depth) and blind hole (500 μm dia, 379 μm depth). Results revealed that the MRR of 1.35 mm^3/min and the smooth machined surface with Ra = 2.824 μm roughness could be achieved under process parameters at 150 mm/s and 8.9 J/cm^2 of scan speed and laser fluence, respectively. A pulsed fiber laser was used to fabricate 3D micro-pattering on alumina and aluminum nitride materials by F. Preusch et al. [16]. The authors found that by applying high pulse overlaps (89 and 84%) and fluence of 64 J/cm^2, higher MRR can be produced while minimum surface roughness of 1.5 μm can be obtained at medium pulse overlapping (42 to 56%). Fabrication of micro-grooves on green ZrO_2 ceramic surfaces using Nd:YAG laser ablation is reported by Yayun Liu et al. [17] wherein the effects of the laser speed, frequency, and power was evaluated on the surface quality and groove dimensions. Results indicated that better surface quality of the grooves with a width of 30–50 μm and a depth of 15–50 μm could be obtained with a frequency below 40 Hz, power below 6 W, and scanning velocity above 200 mm/s. Hanon et al. [18] studied the effects of laser parameters including peak power, pulse duration, focal position, and pulse frequency on the dimensions and microstructure of the micro-holes drilled on alumina ceramic using Nd:YAG laser. Results showed that for a single-laser pulse application, peak power and pulse duration could be effectively used for controlling the crater ablated depth. A full-factorial design and analysis of variance (ANOVA) were applied by Leone et al. [19] to detect the effects of fiber laser parameters on MRR and surface roughness of the pockets

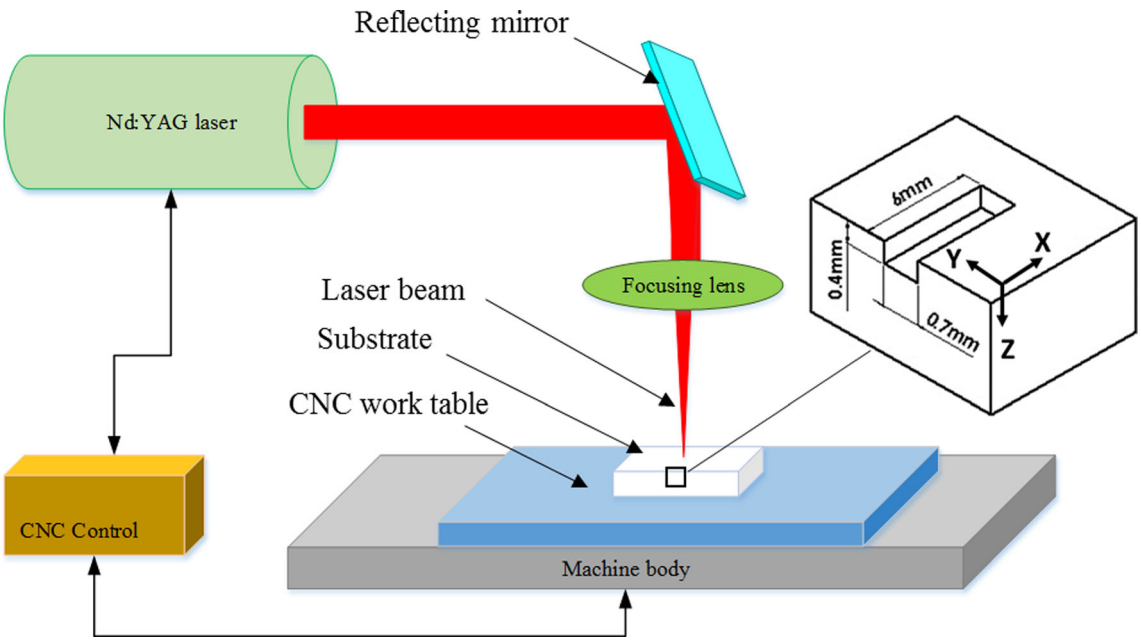

Fig. 1 Schematics of the laser processing setup used in experiments

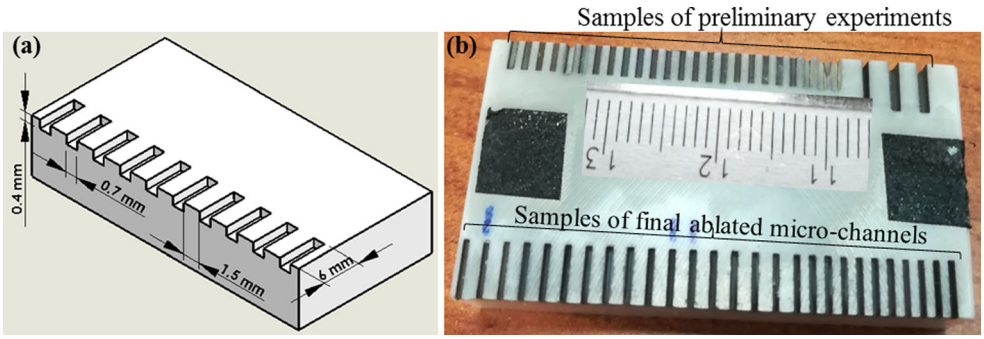

Fig. 2 Laser micro-channels machined on zirconia dental. **a** 3D schematic of micro-channels. **b** Samples of ablated micro-channels

milled on Al_2O_3. The research documented in [20] analyzed the effect of laser parameters on the quality of drilled micro-holes in alumina ceramics. The authors concluded that circularities of the hole at entrance and exit were substantially affected by the hole diameter and laser power, whereas the heat-affected zone and slope/taper of the side walls were influenced by the frequency and laser power.

Regarding the optimization of laser parameters, only few research studies were found in optimizing of laser micro-machining parameters of advanced ceramic materials. Kibria et al. [21, 22] employed gray relational coefficient and response surface methodology to minimize surface roughness and depth variation in laser micro-turning of alumina. Umer et al. [23] applied multi-objective genetic algorithm optimization tool for minimizing the surface roughness and maximizing the MRR of the pockets milled on alumina ceramic by employing Nd:YAG laser process. A gray relational-grade technique was used in to minimize the taperness and HAZ widths of the micro-holes drilled on alumina materials [24] and zirconium ceramic materials [25] by using a pulsed Nd:YAG laser process. Response surface methodology was used as an optimization tool in [26] where authors applied it to minimize the taper and depth deviations of laser micro-grooving ablated on aluminum titanate (Al_2TiO_5). Other research works in the optimization of laser parameters in machining of metals and alloys can be found in [27–30]. Multi-objective particle swarm was applied in the research documented in [27] to optimize laser process parameters while fabricating micro-channels on AISI H13 tool steel. Taguchi methodology along with gray relational analysis method was employed to minimize the HAZ and the redeposited materials of micro-channel fabricated on PMMA using Nd:YAG laser process [28]. Response surface methodology (RSM) was employed to optimize the laser parameters (scanning speed, pulse frequency, and laser intensity) in the research represented in [29]. The authors applied RSM to minimize the micro-channel dimensional errors of various sizes fabricated on Inconel 718 alloys. Regression analysis was performed to minimize micro-pocket surface quality fabricated on titanium alloy sheets using Nd:YVO4 laser [30]. Table 1 summarizes the studies which employed various optimization techniques for optimizing the laser parameters while machining different materials.

From the above literature survey, it can be seen that very few studies have been reported on the micro-machining of zirconia ceramic with no research found in the open literature on the laser micro-channeling of zirconia dental. Furthermore, the effect of laser parameters on the heat-affected zone (HAZ) produced in zirconia has not been investigated before. In the present work, an experimental investigation is conducted on pulsed Nd:YAG laser micro-channeling of zirconia dental with the key focus on minimizing the micro-channel dimensional errors, surface roughness (Ra), and heat-affected zone (HAZ) by employing a multi-objective genetic algorithm (MOGA-II). Three independently controllable input parameters, namely, scanning speed (V), pulse frequency (F), and pulse intensity (I) are considered during the experiments with four levels for each parameters resulting into a total of 64 experiments.

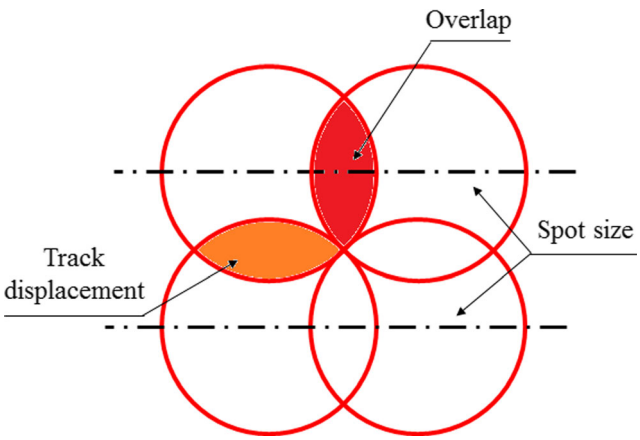

Fig. 3 Schematic of the track displacement, overlap, and spot size

Table 3 Range of the laser input parameters used in the final experiments

Factors	Levels			
	1	2	3	4
Scanning speed (V), mm/s	100	200	300	400
Pulse frequency (F), kHz	5	8	11	14
Pulse intensity (I), %	87	90	93	96

2 Materials and methods

Zirconia dental (Yttria-stabilized zircon, ZrO_2-Y_2O_3) was utilized as the workpiece material from CeramTec Germany. It is a bio-inert ceramics which combines excellent strength and toughness, excellent esthetics, high resistance to corrosion, and absence of allergic reaction [31]. All the zirconia dental samples used in the experiments were of the dimension 50 mm × 50 mm × 10 mm. The chemical composition and mechanical, optical, and thermal properties of as-received zirconia dental material are provided in Table 2.

Lasertec-40 from DMG Mori Sieki was used for machining of the micro-channels. This machine has the capability of producing continuous pulsed waves with a wavelength of 1064 nm, pulse width of 10 μm, and average power of 30 W. The laser setup mainly comprises a Nd:YAG rod which serves as the lasing medium, flashing lamp as a pumping source, and a Q-switch for pulsing. The schematic of the laser setup is illustrated in Fig. 1.

The micro-channel dimensions selected in this study were 6 mm × 0.4 mm × 0.7 mm along X, Y, and Z directions respectively as shown in Fig. 1 which refer to commonly used micro-channel dimensions in micro-fluidics application [32–35]. The micro-channels were machined on the samples such that each adjacent channel was machined at a distance of 1.5 mm from the edge of the previously machined channel as shown in Fig. 2a. The distance of 1.5 mm was selected based on the results of the trial experiments where no overlap of the HAZ was found in the consecutive channels when observed under the scanning electron microscope (SEM). Moreover, a gap of 1.5 mm was also used in a previous study during laser fabrication of micro-channels of similar dimensions in ceramic-based material [36]. This arrangement allows studying the distinct effects of the process parameters without any interference of the thermal effects from the surrounding channels. The 3D schematic of the machined micro-channels and the samples of the micro-channels are presented in Fig. 2a, b respectively.

The experiments were conducted based on full-factorial design, and the analysis of variance (ANOVA) was performed

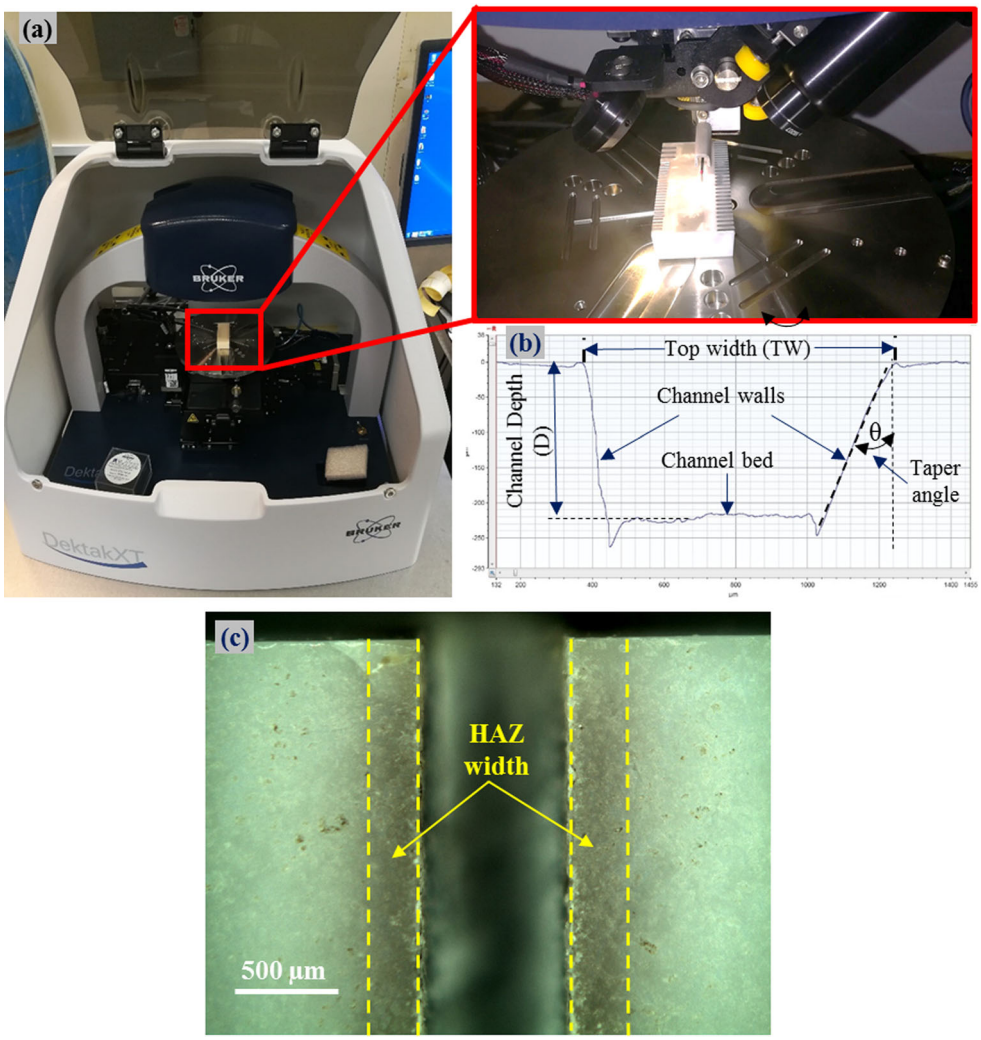

Fig. 4. **a** 3D profilometer (DektakXT Stylus Profiler) used in this study. **b** Typical sample of 2D profile of ablated micro-channel labeled with all geometrical characteristics analyzed in this study. **c** Sample of channel top view shows HAZ

using the Minitab software V17. The primary objective of factorial design and ANOVA tests were to detect the leading effects as well as the interaction of the selected input parameters on the output responses. Three main laser input parameters, namely, scanning speed, pulse intensity, and pulse frequency, were used as the input parameters with four levels each. The scanning speed is defined as the rate of travel of the laser beam on the workpiece, the laser intensity governs the quantity of the heat energy penetrating in the target surface, and the laser pulse frequency controls the number of laser pulses per second. Other laser input parameters were kept constant at appropriate levels. These parameters include the depth of the material removed in one scan (layer thickness = 2 μm), the laser track displacement (10 μm) the offset between the laser spots of the two adjacent scan lines (see Fig. 3), and the diameter of the laser spot size (30 μm). Also, the laser scanning pattern was fixed as random scanning direction [23]. The pulse overlap (see Fig. 3) can be controlled by the spot size, the scanning speed, and the pulse frequency.

Selecting the range of the variable laser input parameters is crucial before performing the actual experiments. Firstly, the ranges of the laser process parameters were selected based on previous studies reported on laser machining of similar bio-materials [15, 17, 19, 37]. Then, preliminary experiments were performed (see Fig. 2b) to decide the actual levels of the process parameters that were later used to conduct the final experiments. It should be noted that the results from the preliminary experiments showed that the intensity values lower than the 87%, the frequencies higher than 14 kHz, and the scanning speed above 400 mm/s produce very low energy per unit area resulting in no ablation. On the other hand, the scanning speed lower than 100 mm/s, the pulse frequency less than 5 kHz, and the pulse intensity higher than 96% result in uncontrollable material removal due to an excessive increase in the energy per unit area and increase the dimensional errors and surface roughness. The selected levels of the laser input parameters for the final experiments are presented in Table 3.

The ablated micro-channels' geometries and the surface roughness were measured by using a 3D profilometer (DektakXT Stylus Profiler) from Bruker, USA, equipped with an inductive gauge of 12.5 μm radius diamond stylus (see Fig. 4a). To capture the 2D profile of the micro-channel, ten profiles were scanned at random locations across the length of the channel with a resolution of 0.03 μm and scanning speed of 5 μm/s. Then, the average of ten scanned profiles was used to measure the depth (D), top width (TW), taper angles (θ), and the surface roughness (Ra). Figure 4b shows a typical sample of the 2D profile of machined micro-channel labeled with all geometrical characteristics (D, TW, and θ). Later, the depth error (DE) and the top width error (TWE) and the taper angle (θ) were analyzed to evaluate the channel dimensions. DE and TWE were calculated by using Eqs. (1) and (2), respectively:

$$\mathrm{DE} = |DD - D| \tag{1}$$

$$\mathrm{TWE} = |DTW - TW| \tag{2}$$

where DD is the desired depth (400 μm), D is the actual depth measured after machining, DWT is the desired top width

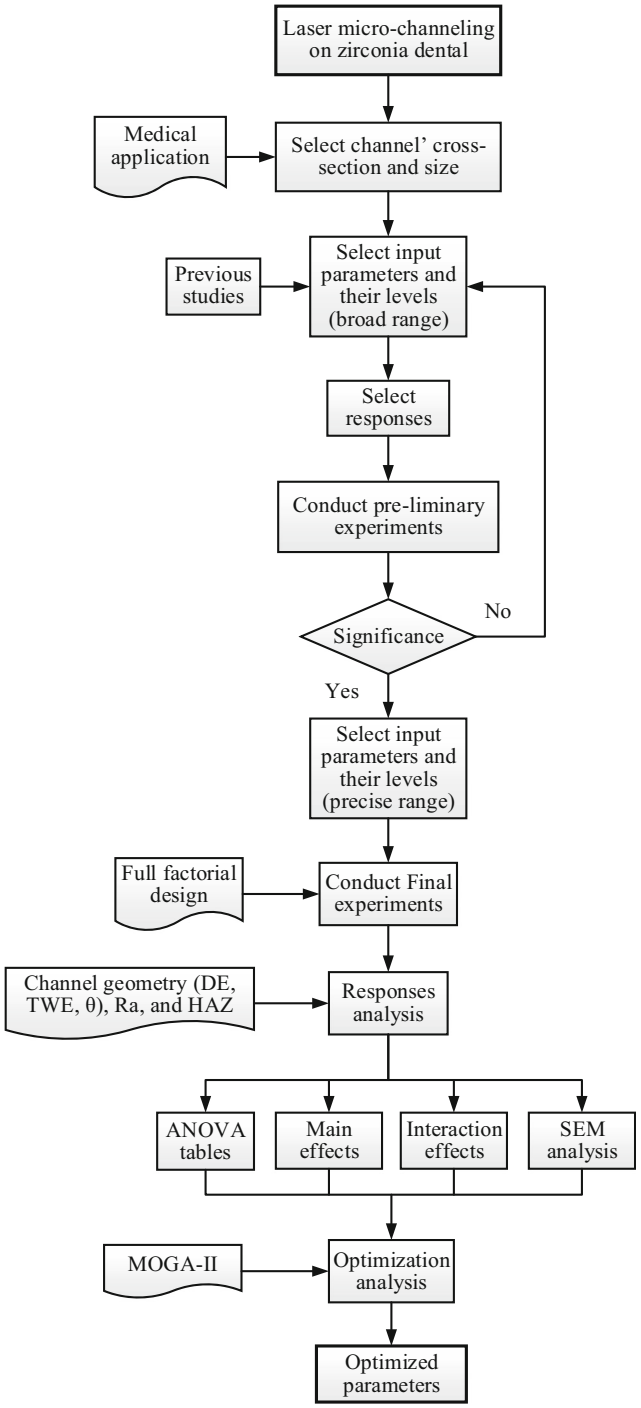

Fig. 5 Research methodology

Table 4 DOE runs for the experimental plan

Exp. no.	Input parameters			Responses				
	V (mm/s)	F (kHz)	I (%)	DE (μm)	TWE (μm)	θ (^{0})	R_a (μm)	HAZ (μm)
1	200	11	87	298.5	5.0	17.23	7.16	55.45
2	400	8	87	335.0	86.4	13.7	8.23	39.17
3	400	11	90	201.3	4.7	14.3	4.21	65.14
4	200	14	87	287.9	69.7	17.36	6.15	49.21
5	100	14	96	363.8	142.1	19.45	2.13	92.7
6	300	5	87	311.6	9.9	17.4	6.56	68.84
7	300	14	87	320.2	6.5	19.25	5.96	54.8
8	400	14	93	206.6	56.4	15.05	4.07	81.26
9	200	8	96	87.9	62.4	13.85	2.7	91.7
10	200	14	96	84.4	56.5	19.32	3.67	136.7
11	200	11	90	198.8	62.9	15.78	4.33	91.51
12	400	11	87	343.7	58.0	14.15	8.56	35.21
13	400	5	96	127.7	45.8	18.25	2.65	132.2
14	100	11	90	21.5	96.5	12.25	3.32	101.82
15	100	8	90	45.1	85.6	11.35	3.95	109.42
16	100	8	87	201.1	139.8	7.52	4.85	95.31
17	400	5	87	330.9	56.4	12.45	7.87	61.32
18	300	8	93	237.0	9.4	12.35	5.2	60.65
19	100	5	93	361.0	191.6	13.7	3.01	121.25
20	100	14	93	292.1	121.3	17.65	4.32	112.21
21	400	11	96	147.7	53.2	17.5	2.86	125.94
22	300	8	96	90.4	2.4	12.54	2.96	98.74
23	200	5	90	203.5	56.3	14.25	4.84	95.21
24	400	8	90	198.5	52.1	15.25	3.95	57.1
25	400	14	87	245.3	78.5	16.55	2.95	37.21
26	300	5	96	56.8	12.5	17.56	3.25	95.94
27	200	11	96	107.9	51.9	18.25	2.92	75.85
28	300	11	93	195.6	20.5	13.6	2.45	119.6
29	400	5	93	189.4	19.5	14.21	4.51	99.9
30	400	8	96	136.8	50.1	12.53	2.78	77.65
31	100	11	96	301.7	148.0	20.1	2.42	161.17
32	400	14	96	159.7	61.9	12.15	2.44	127.95
33	200	14	93	93.5	62.2	16.25	4.12	102.2
34	200	8	93	173.5	56.9	16.05	4.67	70.9
35	100	8	93	345.2	189.9	17.85	2.39	90.7
36	100	14	87	241.1	109.8	17.32	4.85	109.9
37	200	5	93	50.2	96.2	15.77	3.45	98.5
38	300	8	90	157.5	69.5	19.65	3.69	95.32
39	300	8	87	311.2	13.5	16.25	5.54	109
40	200	5	96	77.9	85.9	17.25	2.85	102.87
41	400	5	90	184.3	12.9	17.62	3.94	67.91
42	100	11	93	321.0	161.9	25.5	3.13	100.1
43	200	5	87	208.5	41.0	11.35	5.17	69.84
44	300	5	90	130.8	20.5	15.21	3.78	59.82
45	400	14	90	220.4	53.6	15.3	2.41	59.54
46	300	5	93	218.2	18.2	11.15	6.11	109.82
47	200	8	90	192.8	21.0	9.8	3.93	124.85

Table 4 (continued)

Exp. no.	Input parameters			Responses				
	V (mm/s)	F (kHz)	I (%)	DE (μm)	TWE (μm)	θ (^{0})	R_a (μm)	HAZ (μm)
48	200	11	93	82.3	76.2	17.55	3.94	63.1
49	100	5	87	201.1	139.8	14.35	4.31	100.97
50	300	11	87	318.2	2.1	15.24	5.21	75.85
51	300	14	93	126.5	6.7	13.2	3.8	114.7
52	100	11	87	201.5	125.4	18.25	4.95	73.6
53	400	11	93	209.4	20.5	13.55	5.42	59.95
54	100	5	96	445.3	159.1	16.45	3.35	155.3
55	200	8	87	226.6	70.7	16.45	5.47	43.6
56	200	14	90	249.9	26.3	16.24	4.57	167.45
57	100	8	96	385.1	85.1	15.15	2.9	174.24
58	100	14	90	1.5	116.5	12.65	3.52	95.4
59	300	14	96	77.0	8.8	15.2	3.25	125.85
60	300	11	90	173.1	30.5	16.84	3.29	79.67
61	100	5	90	27.5	96.5	15.25	3.49	115.21
62	300	14	90	170.4	59.5	14.24	3.57	88.55
63	400	8	93	196.6	16.4	18.54	3.84	74.85
64	300	11	96	96.8	102.5	16.94	3.87	65.35

(700 μm), and *TW* is the actual top width measured after machining. The taper angle (θ) was defined as the slope between the side wall of the channel and the normal to the channel bed (see Fig. 4b). Arithmetic mean surface roughness (R_a) was evaluated directly at the bottom of each of the ten profiles (channel bed, see Fig. 4b), and the averaged value from the ten profiles was used for further analysis. Heat-affected zone (HAZ) has important influence on the micro-channeling of the zirconia dental ceramics, which can induce the forming of micro-cracks on the surface which will poorly affect the bonding process in micro-fluidic devices. It is formed around the channels by the reasons of the laser with high energy density, vapor blast ejections of melts ceramics, and rapid condensation [11, 17]. Therefore, it is necessary to control the production of heat-affected zone. In this study, optical microscopic (mikroskop technik rathenow from Askania Co.) is used to measure the average HAZ width at different laser parameters. Figure 4c illustrates the diagram of the measure of the HAZ width which can be visualized surrounding the micro-channels.

Scanning electron microscope (SEM) from JEOL, Japan (Model JSM–7600F) was utilized to conduct the surface

Table 5 ANOVA table for depth error (DE) and top width error (TWE)

Source	DF	Depth Error (DE)				Top width error (TWE)			
		Adj SS	Adj MS	F-Value	*P* Value	Adj SS	Adj MS	F-Value	*P* value
Model	36	2,420,425	67,234	70.73	*0.000*	266,298	7397.2	5.26	*0.000*
Linear	9	2,006,959	222,995	234.59	*0.000*	225,926	25,102.9	17.83	*0.000*
V	3	1,231,234	410,411	431.74	*0.000*	212,084	70,694.8	50.22	*0.000*
F	3	7772	2591	2.73	0.064	2803	934.5	0.66	0.582
I	3	767,954	255,985	269.29	*0.000*	11,039	3679.6	2.61	0.072
Two-way interactions	27	413,466	15,314	16.11	*0.000*	40,372	1495.3	1.06	0.438
V × F	9	7657	851	0.90	0.543	9480	1053.4	0.75	0.663
V × I	9	397,831	44,203	46.50	*0.000*	21,758	2417.6	1.72	0.133
F × I	9	7978	886	0.93	0.514	9133	1014.8	0.72	0.686
Error	27	25,666	951			38,005	1407.6		
Total	63	2,446,091				304,303			

Table 6 ANOVA table for taper angle (θ) and surface roughness (Ra)

Source	DF	Taper angle (θ)				Ra			
		Adj SS	Adj MS	F-Value	P value	Adj SS	Adj MS	F-Value	P value
Model	36	367.965	10.221	1.88	*0.047*	109.321	3.0367	3.86	*0.000*
Linear	9	83.615	9.291	1.70	0.137	82.469	9.1632	11.66	*0.000*
V	3	7.220	2.407	0.44	0.725	7.856	2.6188	3.33	*0.034*
F	3	52.791	17.597	3.23	*0.038*	1.995	0.6650	0.85	0.481
I	3	23.604	7.868	1.44	0.252	72.618	24.2059	30.79	*0.000*
Two-way interactions	27	284.350	10.531	1.93	*0.046*	26.852	0.9945	1.26	0.273
V × F	9	64.099	7.122	1.31	0.279	14.148	1.5720	2.00	0.079
V × I	9	141.202	15.689	2.88	*0.016*	8.706	0.9673	1.23	0.318
F × I	9	79.050	8.783	1.61	0.162	3.998	0.4442	0.57	0.813
Error	27	147.153	5.450			21.227	0.7862		
Total	63	515.118				130.548			

morphology analysis. Methanol was used to clean the debris from the ablated micro-channels before the SEM analysis. Since ceramics do not respond well to the electron beam for forming the image in SEM, the platinum coating was applied to the machined sample to improve their visibility during the surface morphology analysis. Figure 5 shows the research methodology followed in the current study.

3 Results and analysis

Table 4 shows the experimental results of 64 runs obtained from full-factorial design for the selected input parameters and the corresponding output responses.

Table 7 ANOVA table for heat-affected zone (HAZ)

Source	DF	HAZ			
		Adj SS	Adj MS	F-Value	*P* value
Model	36	50,234	1395.4	3.04	*0.002*
Linear	9	32,005	3556.2	7.74	*0.000*
V	3	11,875	3958.3	8.61	*0.000*
F	3	2020	673.3	1.46	0.246
I	3	18,111	6036.9	13.13	*0.000*
Two-way interactions	27	18,228	675.1	1.47	0.162
V × F	9	4881	542.4	1.18	0.346
V × I	9	10,305	1145.1	2.49	*0.032*
F × I	9	3041	337.9	0.74	0.674
Error	27	12,410	459.6		
Total	63	62,644			

3.1 ANOVA and response surfaces results

The ANOVA test was performed to check the significance of the laser input parameters (V, F, I) on the output responses including DE, TWE, θ, Ra, and HAZ. The ANOVA results for the selected outputs are shown in Tables 5, 6 and 7. For each input parameter or the combination of the input parameters, the ANOVA tables list (i) the degrees of freedom (DF), (ii) the adjusted sum of squares (Adj SS), (iii) the adjusted mean squares (Adj MS), (iv) the F-value, and (v) the *p* value. During the ANOVA, the significance of the parameters or their combinations was accessed based on the *p* value. The ANOVA was conducted with a confidence interval of 95% ($\alpha = 0.05$). Therefore, an input parameter or its interaction was regarded as significant if the *p* value was < 0.05. The normality of the residuals was checked graphically to satisfy the conditions of the ANOVA [38]. To enhance the readability of the ANOVA tables, the *p* value of the significant input parameters or their interactions has been presented in the italic text. It should be noted that no third-order interactions of the input parameters had any significant effect on any of the

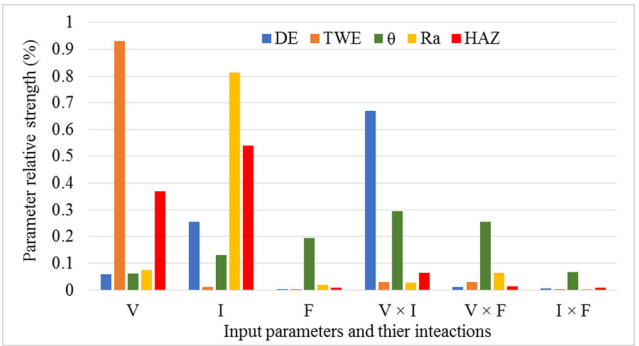

Fig. 6 ANOVA spline relative strength of input variables and their interactions for all responses

outputs, and these were not considered in the analysis. The results of ANOVA regarding the channel dimensional accuracy indicate that the depth error (DE) is affected by scanning speed (V) and pulse intensity (I) and their interactions (V × I) as shown in Table 5. This is due to the reason that when the material is irradiated at various scanning speeds and different

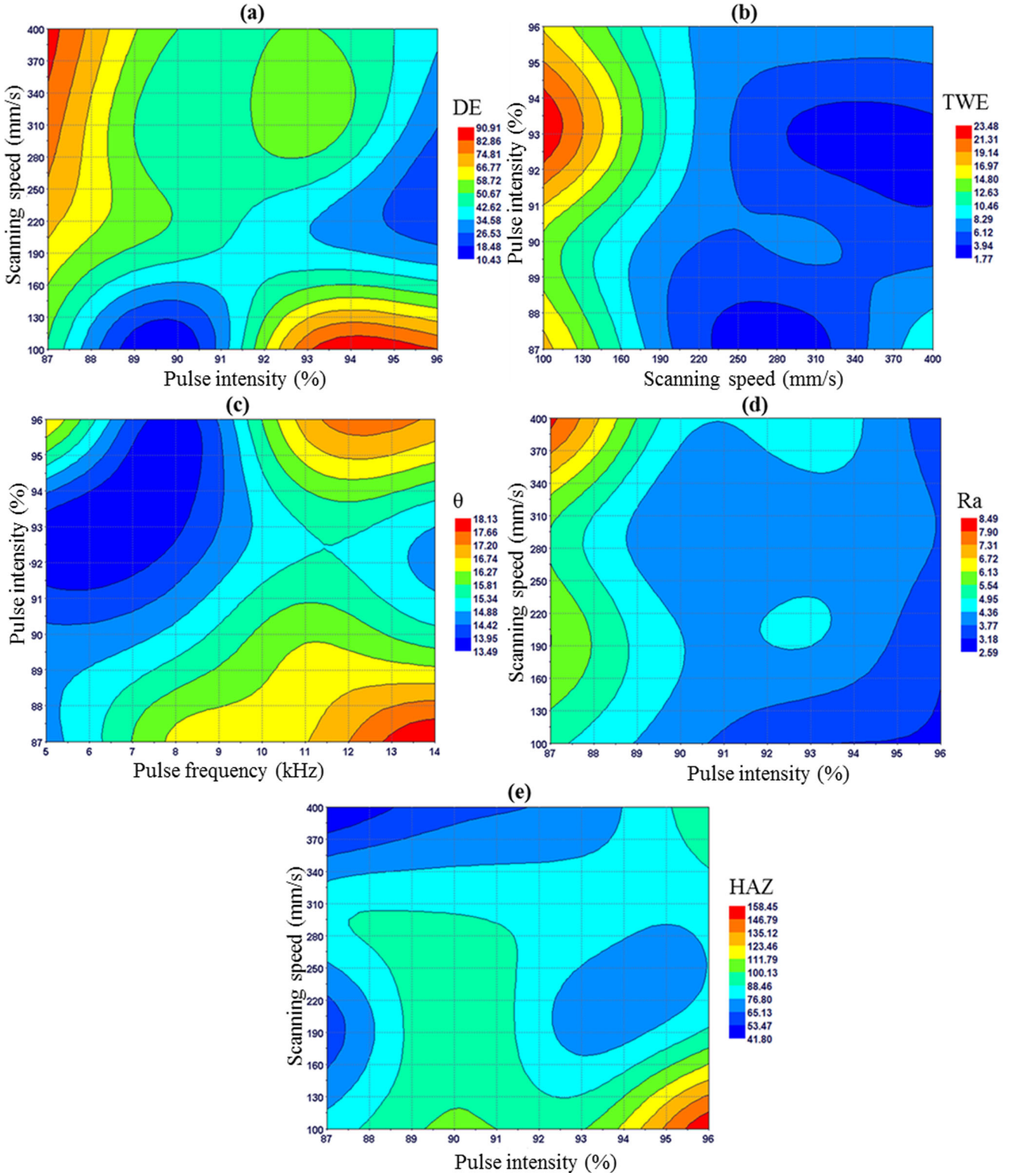

Fig. 7 Response surface plots, effects of the indicated process parameters on the **a** depth error (DE), **b** width error (TWE), **c** taper angle (θ), **d** surface roughness (Ra), **e** heat-affected zone (HAZ)

pulse intensities, the available energy and temperature required to melt and vaporize the material varies. This causes a significant variation in the ablated depths [3, 39]. On the other hand, the top width error (TWE) is affected only by the scanning speed (Table 5) while neither the scanning speed nor the pulse intensity has effects on the taper angle (θ) as a single factor. However, the interaction of the scanning speed and pulse intensity have significant effect on θ as depicted in Table 6. This is because when the machined depth goes deeper at high laser intensity and low scanning speed, the laser looses its energy and it becomes difficult to eject the fused mass effectively, which reduces the bottom width and as a result

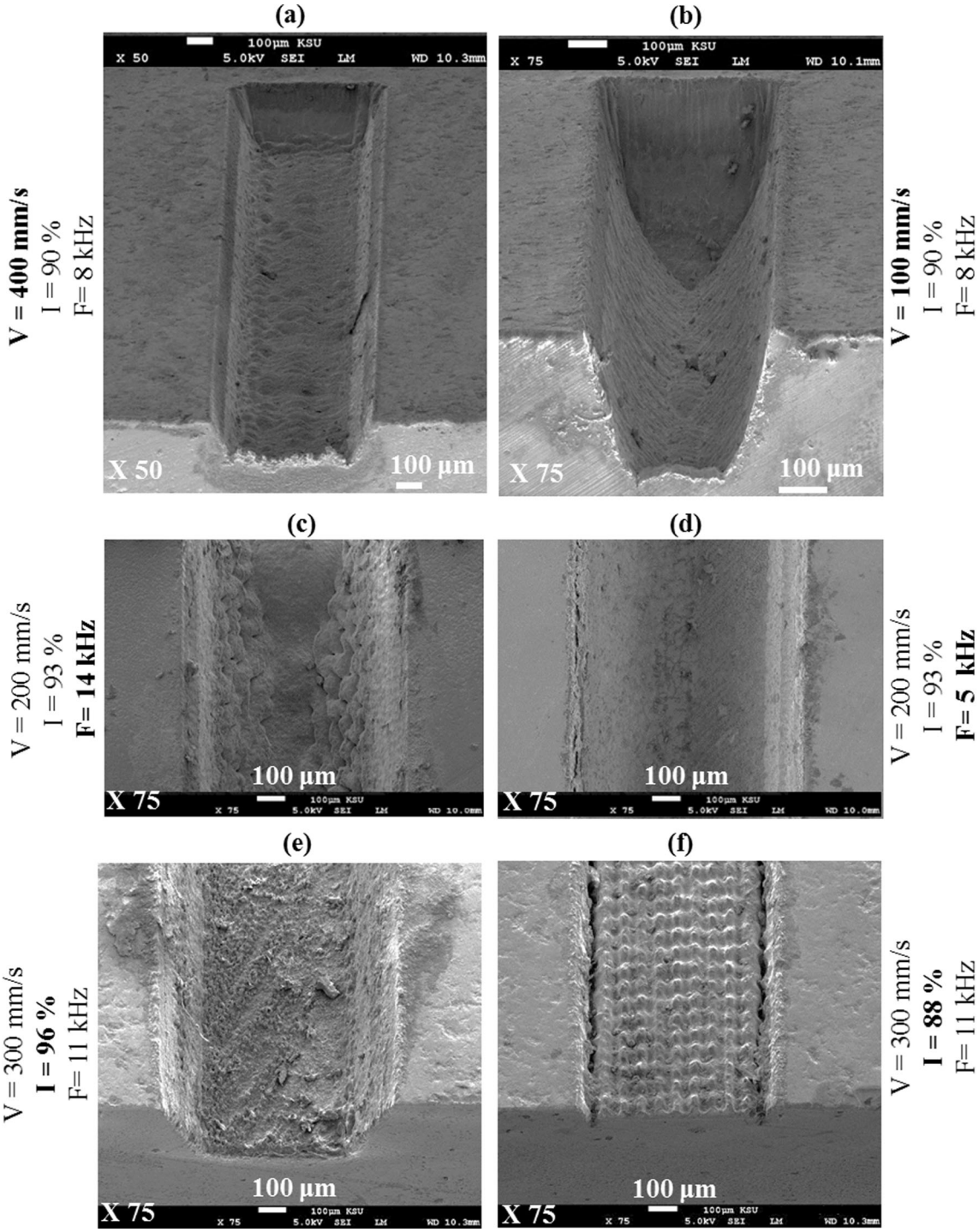

Fig. 8 SEM micrographs of the micro-channels ablated at **a**, **b** high and low levels of scanning speed (V), **c**, **d** high and low intensity levels of pulse frequencies (F), and **e**, **f** high and low levels of the pulse intensity (I)

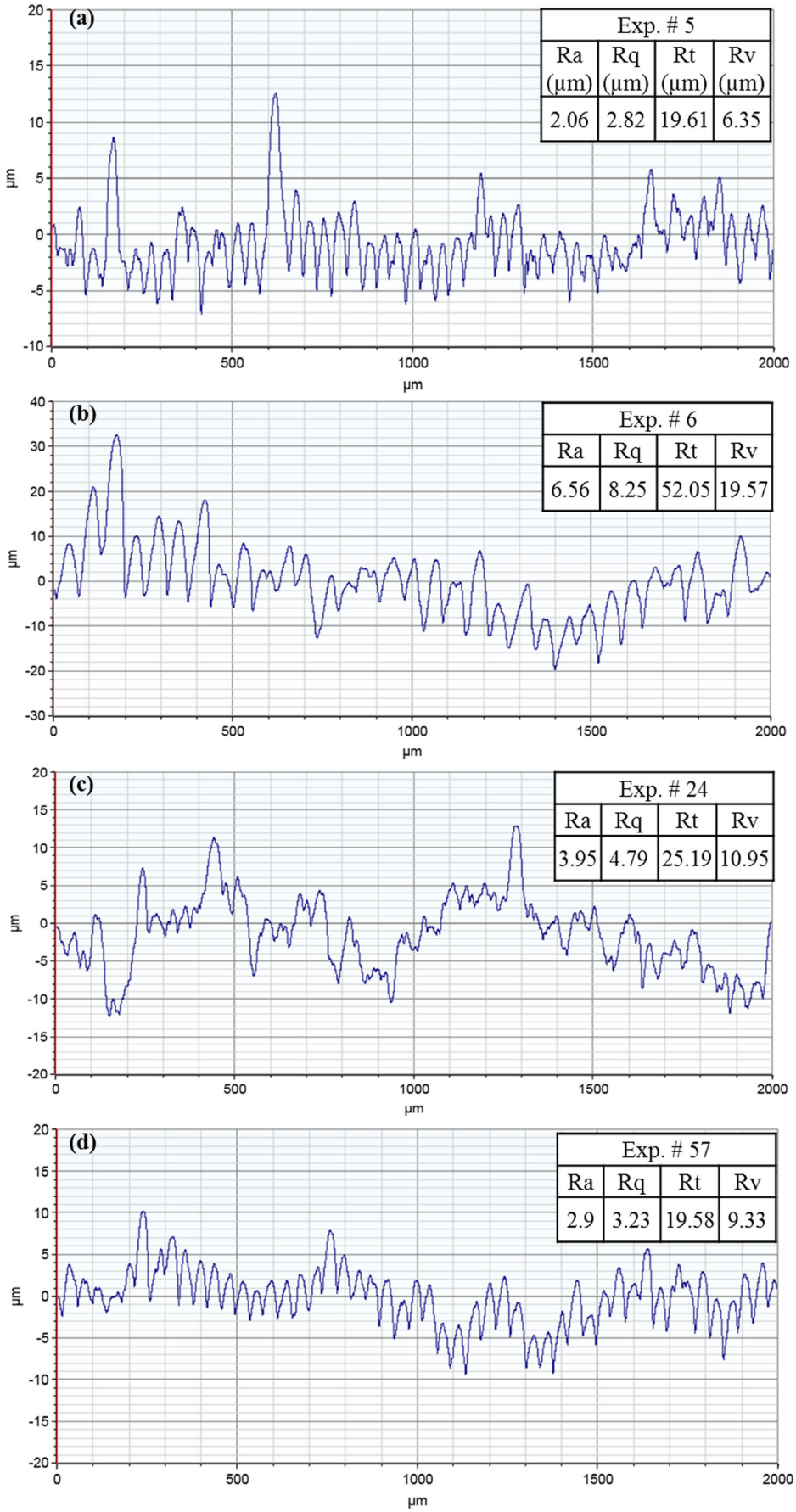

Fig. 9 Surface roughness profile of **a** Exp. no. 5, **b** Exp. no. 6, **c** Exp. no. 24, and **d** Exp. no. 57

increases the taper angle [36]. Moreover, pulse frequency has significant effect on taper angle (θ) (Table 6). The results of ANOVA concerning the surface roughness (Ra) and HAZ specify that V and I have a significant influence on both Ra and HAZ (Tables 6 and 7). The low laser energy caused more unmolten materials accumulated at the bottom and walls of the ablated channel which makes the channel surface rougher. Moreover, at higher pulse intensity (I) and lower scanning speed (V), the HAZ width increases due to increase in the surface temperature of the substrate. Furthermore, the HAZ was found to be affected by the interaction (V × I) as shown in Table 7.

The ANOVA tables are valuable tools for identifying the statistical importance of the selected input parameters and their interactions. Nevertheless, the ANOVA does not contribute towards quantifying the relative effect of input parameters on the output responses. These aspects can be analyzed by using the ANOVA spline relative strength (Fig. 6) and response surfaces (Fig. 7). Figure 6 shows the relative strength of the significant input parameters and their interactions as computed by using the means of smoothing spline ANOVA in Mode Frontier® software for DE, TWE, θ, Ra, and HAZ. Figure 7 demonstrates the response surfaces using radial basis functions which show how the most significant input parameters affect all responses.

As can be seen in Fig. 6, the pulse intensity (I), the scanning speed (V), and their interaction (V × I) are the most dominant factors affecting the depth error (DE) as their relative strength values are higher compared to other input parameters. It is evident that the minimum depth of error can be found at moderate levels of scanning speed (200–300 mm/s) and low levels of pulse intensity (89–90%) as shown in Fig. 7a. The worst value of DE (> 90 μm) is obtained at higher levels of I and V (Fig. 7a). The 3D views of SEM images (Fig. 8a, b) show that there are sound changes in the ablated depth of the micro-channels machined at high and levels of scanning speed when other input parameters are kept constant. This is because high scanning speed leads to the reduction in the target material surface temperature which leads to obtaining undersized depth. In contrast, low scanning speed leads to an increase in laser efficiency which results in ablating oversized depth [15]. Among all input parameters, the scanning speed was found to be the most significant factor affecting the top width error (TWE), whereas other input parameters show the negligible effect on TWE as elaborated in Fig. 6. The TWE is at minimum at moderate scanning speed as displayed in Fig. 7b. The taper angle (θ) of the machined micro-channels is affected by all input parameters (V, I, and F) and their interactions. The effect of pulse frequency (F) is considerably higher in comparison with the pulse intensity and scanning speed. Figure 7c shows that taper angle increases with increasing pulse frequency. This is attributed to the fact that as the pulse frequency increases, the pulse overlap decreases and this leads to decrease in laser energy which results in less bottom depth to be ablated and consequently obtaining high taper angle (see Fig. 8c, d). Figure 6 shows that the pulse intensity mostly controls the surface roughness (Ra). Ra increases with decreasing of pulse intensity as shown in Fig. 7d. This is due to the reason that at lower pulse intensity, the mean temperature of the ablated channels decreases and hence the molten material decrease, which leads to a rougher channel surface [40], as shown in Fig. 8. In contrast, at high pulse intensity, the higher temperature achieved on the target surface, the higher the molten materials are which results in smooth surfaces (Fig. 8f). Overall, the optimal area of Ra (minimum Ra) corresponds to high pulse intensity and low scanning speed [37]. The surface roughness profile of the micro-channels ablated at different parametric combinations is shown in Fig. 9a–d. It is obvious that the roughness profiles vary with the variation of the laser input parameters. For instance, the value of Ra increases from 2.06 μm at high pulse intensity (I) of 96% (see

Table 8 Optimization model used for the study

Objective functions	1. Minimize depth error (DE) 2. Minimize heat affected zone (HAZ)
Constraints	1. Top width error (TWE) < 12.0 μm 2. Taper angle (θ) < 16.0° 3. Surface roughness (Ra) < 6.0 μm

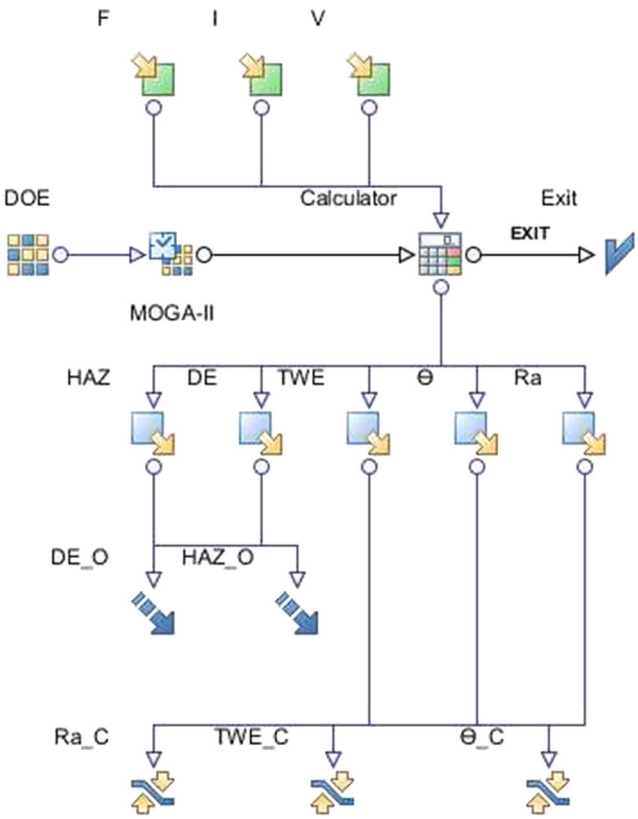

Fig. 10 Optimization process-flow using MOGA-II

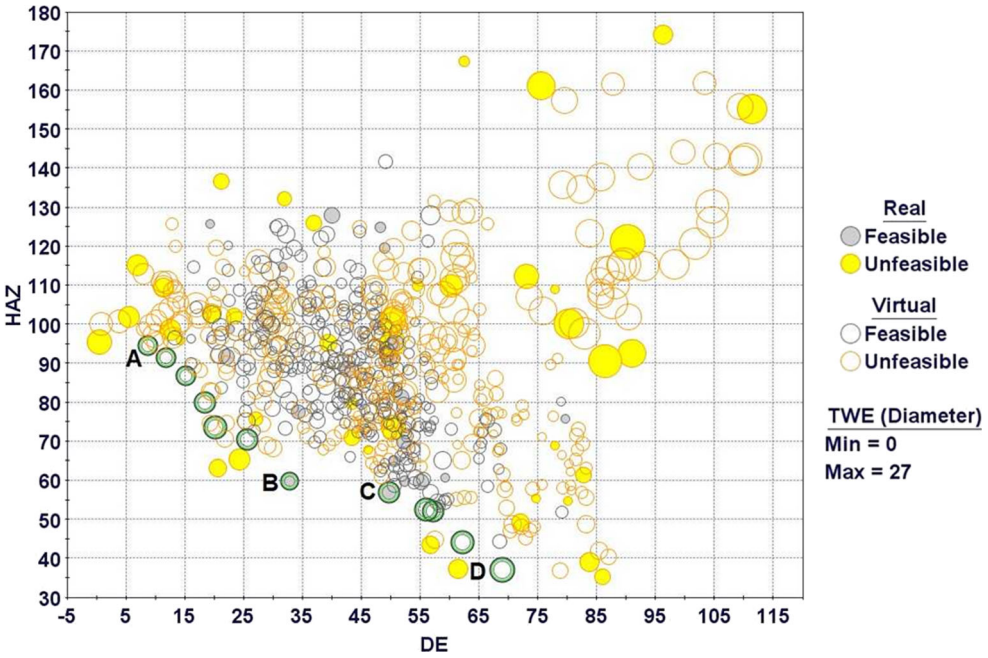

Fig. 11 A 3D bubble chart showing the design points obtained with the output variable of TWE (A, B, C, D are some of the selected optimal points)

Fig. 9a) to reach 6.56 μm at low I of 88% as shown in Fig. 9b. On the other hand, the value of Ra decreases from 3.95 to 2.9 μm when the scanning speed decreases from 400 to 100 mm/s as presented in Fig. 9c, d. Finally, the heat-affected zone (HAZ), as expected, is highly dependent on pulse intensity and scanning speed and their interaction (V × I) (see Fig. 6). As shown in the Fig. 6, the effect of pulse intensity is higher as compared to the scanning speed. The maximum value of HAZ can be found at a higher intensity and lower scanning speed (Fig. 7e). It is also pronounced that the HAZ width is significantly high and clearly visible at a higher intensity (Fig. 8e) compared to at low intensity (Fig. 8f) in which the HAZ is very difficult to be observed. The is because the high pulse intensity generates high thermal energy, which produces higher HAZ width [24].

3.2 Optimization results

The optimization problem is expressed to minimize the depth error (DE) and heat-affected zone (HAZ) width of the ablated micro-channels at a time. The optimization algorithm utilized the response surfaces based on radial basis functions to predict

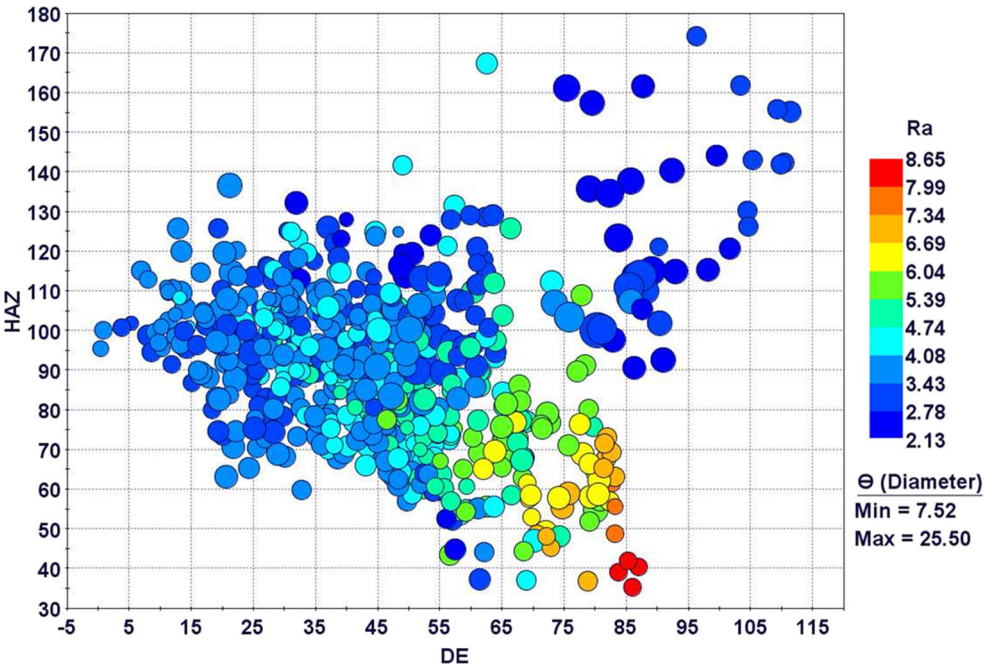

Fig. 12 A 4D bubble chart showing the design points obtained with variables of DE, HAZ, Ra, and taper angle

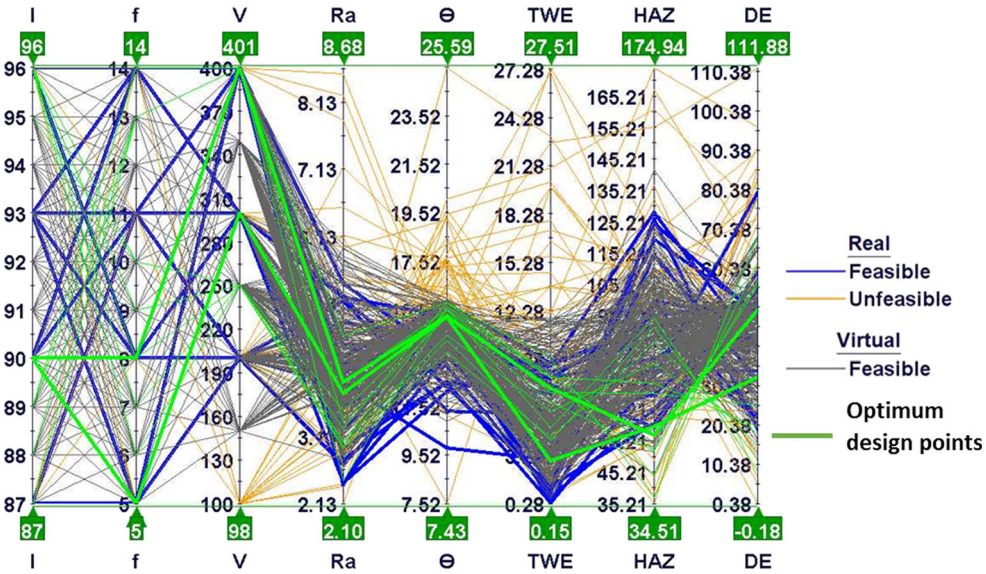

Fig. 13 A parallel coordinate chart for the analysis of laser micro-milling parameters

responses for a particular design point. The upper limits are set for the remaining output parameters as constraints. Top width error greater than 12 μm, taper angle more than 16°, and surface roughness (Ra) greater than 6 μm are regarded as an unfeasible solution in the optimization. The Ra value of 6 μm was selected based on the requirement of the femoral heads and cups made from zirconia and is considered to be sufficient to ensure long-term stability of the implants [41, 42]. The other constraint values were taken such that the overall optimization problem should be completed with the proposed methodology in a reasonable amount of time. If more tight values of the constraints were selected, most of the runs would be found unfeasible, and the problem would be computationally costly. On the other hand, the too relaxed constraint would make the choice of the optimal solution more difficult. The optimization model (i.e., objective functions and the constraints) is represented in Table 8. The process flow for the optimization problem is developed using Mode Frontier® program as depicted in Fig. 10.

MOGA-II (Multi-objective genetic algorithm-II) is selected for the optimization problem. It is based on a new multi-search elitism method that improves its efficiency. This new search method can preserve some better solutions and avoid premature convergence to local optima. Most of the MOGA-II parameters are internally set by the optimization program, and the user has to put few basic parameters. The total number of design points are equal to the product of no. of generations and number of design points in the DOE table. More information regarding MOGA-II can be found in [43].

A total of 700 generations has been processed using MOGA-II. The design points obtained are shown in Figs. 11 and 12 using bubble charts. The real design points correspond to the experimental runs, and the response surfaces predict the virtual runs.

Figure 11 shows the total design points expressed relative to the two objective functions, i.e., depth error (DE) and heat-affected zone (HAZ). The top width error (TWE) is signified by the size of the bubbles. It is clearly evident that high DE and higher HAZ corresponds to higher TWE obtained and vice versa. The design points with the lowest DE have moderate intensities, low scanning speed, and higher frequencies. Similarly, lower HAZ is obtained with low-intensity values, higher scanning speeds, and moderate to high frequencies. The top right area with high DE and HAZ is characterized by higher intensities, low to moderate frequencies, and lower scanning speeds. Since the aim of the optimization study is to minimize the DE and the HAZ, the design points corresponding to the lower left area of the bubble chart will be chosen for the optimal solutions. A Pareto-front can be marked in Fig. 11 connecting the optimal design points from A to D.

Table 9 Optimum design points

ID	Scanning speed (mm/s)	Pulse intensity (%)	Pulse frequency (kHz)	Depth error (μm)	Top width error (μm)	Taper angle (θ)	Ra (μm)	HAZ (μm)
A	250	96	6	8.60	5.02	15.55	3.06	94.60
B	300	90	5	32.70	2.93	15.21	3.78	59.82
C	400	90	8	49.62	7.44	15.25	3.95	57.10
D	400	87	13	68.85	9.33	15.83	4.63	37.17

Figure 12 shows four variables at a time using a 4D bubble chart. Here, the diameter of the bubbles represents taper angle (θ) whereas the colors represent the surface roughness (Ra). The effect of Ra on DE is clearly demonstrated in the 4D chart as the high Ra area corresponds to higher DE. These design points are characterized by low intensities, high scanning speed, and moderate frequencies. Similarly, low HAZ corresponds to higher Ra and low to moderate taper angle. The top right area of Fig. 12 contains design points with low Ra and moderate taper angle. They are associated with high intensities, low scanning speed, and moderate frequencies. In general, taper angle variation is not high, and most of the values lie in between 13 and 18°. This can be visualized by variation in the size of the bubbles in Fig. 12.

The relationships between all input and output variables can be visualized using a parallel coordinate chart as shown in Fig. 13. Most of the unfeasible design points are linked to extreme intensities, low scanning speed, and high pulse frequency leading to high HAZ and high depth error. Optimum results are found with moderate intensities and scanning speed and low frequencies. Some of the optimal design points are listed in Table 9. Out of the four optimal design points, the design points B and C are real and correspond to the original DOE matrix.

It can be concluded from the above discussions that the laser intensity mostly controls the channel's depth dimensional accuracy and heat-affected zone, followed by scanning speed and pulse frequency. This observation is matched with the results obtained by ANOVA (see Fig. 6). To get good dimensional accuracy and low HAZ for deeper channels, low to moderate intensity could be selected with a higher number of laser scan. Higher scanning speeds result in poor surface finish but give low HAZ values. The effect of frequency is not straightforward but for the designed micro-channels, low to moderate frequencies are recommended.

4 Conclusions

In the present paper, an experimental study based on design of experiments (DoE) was carried out for fabricating micro-channels in zirconia dental by using Nd:YAG pulsed laser. ANOVA tables, response surfaces, and SEM micrographs were used to analyze the effects of key input laser parameters on the dimensional accuracy and the surface quality of the ablated micro-channels. Moreover, multi-objective genetic algorithm (MOGA-II) optimization was applied to minimize the ablated depth error (DE) and the heat-affected zone (HAZ) of the micro-channels. Based on the overall analysis, the following conclusions can be drawn:

- The channel dimensional error (DE and TWE) are mostly influenced by laser beam scanning speed, pulse intensity, and the interaction between them.
- The effect of pulse frequency is significant on the taper angle, and its effects are negligible on DE and TWE. However, the effect of pulse frequency is minimal as compared to the scanning speed and pulse intensity.
- The surface roughness (Ra) is mainly controlled by laser scanning speed and laser pulse intensity. Ra is directly proportional to scanning speed and inversely proportional to pulse intensity.
- The heat-affected zone (HAZ) width increases with increasing of substrate temperature that is at higher pulse intensity and lower scanning speed.
- Multi-objective optimization is successfully carried out by the MOGA-II algorithms, and the optimized solutions are consistent with the ANOVA results. However, laser micro-milling is a complicated process, and it is not easy to find the proper combination of process parameters to achieve different quality outputs.
- Optimal solutions are characterized by moderate intensity values. For good dimensional accuracy and low Ra, low scanning speeds and pulse frequencies are recommended. In contrast, lower HAZ values are obtained with higher scanning speeds and frequencies.
- The current study provides the optimized sets of laser parameters that can be employed for the fabrication of the micro-channels with high dimensional accuracy, minimum heat-affected zone, and acceptable surface finish for several biomedical applications.

Acknowledgements This work was supported by the Deanship of Scientific Research, King Saud University, through Vice Deanship of Scientific Research Chairs.

References

1. Groß GA, Thelemann T, Schneider S, Boskovic D, Köhler JM (2008) Fabrication and fluidic characterization of static micromixers made of low temperature cofired ceramic (LTCC). Chem Eng Sci 63:2773–2784. https://doi.org/10.1016/j.ces.2008.02.030
2. Malecha K, Golonka LJ (2009) Three-dimensional structuration of zero-shrinkage LTCC ceramics for microfluidic applications. Microelectron Reliab 49:585–591. https://doi.org/10.1016/j.microrel.2009.02.020
3. Samant AN, Dahotre NB (2009) Laser machining of structural ceramics—a review. J Eur Ceram Soc 29:969–993. https://doi.org/10.1016/j.jeurceramsoc.2008.11.010
4. Das S, Doloi B, Bhattacharyya B (2016) Fabrication of stepped hole on zirconia bioceramics by ultrasonic machining. Mach Sci Technol 20:681–700. https://doi.org/10.1080/10910344.2016.1224016
5. Abdo BMA, Darwish SM, Al-Ahmari AM, El-Tamimi AM (2013) Optimization of process parameters of rotary ultrasonic machining

based on Taguchi's method. Adv Mater Res 748:273–280. https://doi.org/10.4028/www.scientific.net/AMR.748.273
6. Abdo BMA, Darwish SM, El-Tamimi AM (2012) Parameters optimization of rotary ultrasonic machining of zirconia ceramic for surface roughness using statistical taguchi's experimental design. Appl Mech Mater 184–185:11–17. https://doi.org/10.4028/www.scientific.net/AMM.184-185.11
7. Chang CW, Kuo CP (2007) Evaluation of surface roughness in laser-assisted machining of aluminum oxide ceramics with Taguchi method. Int J Mach Tools Manuf 47:141–147. https://doi.org/10.1016/j.ijmachtools.2006.02.009
8. Dandekar CR, Shin YC, Barnes J (2010) Machinability improvement of titanium alloy (Ti-6Al-4V) via LAM and hybrid machining. Int J Mach Tools Manuf 50:174–182. https://doi.org/10.1016/j.ijmachtools.2009.10.013
9. Ahmed N, Darwish S, Alahmari AM (2016) Laser ablation and laser-hybrid ablation processes: a review. Mater Manuf Process 31:1121–1142. https://doi.org/10.1080/10426914.2015.1048359
10. Mishra S, Yadava V (2015) Laser beam micromachining (LBMM)—a review. Opt Lasers Eng 73:89–122. https://doi.org/10.1016/j.optlaseng.2015.03.017
11. Kim J, Xu X (2003) Excimer laser fabrication of polymer microfluidic devices. J Laser Appl 15:255–260. https://doi.org/10.2351/1.1585085
12. Schreck S, Gahr K Zum (2005) Laser-assisted structuring of ceramic and steel surfaces for improving tribological properties. Appl Surf Sci 247:616–622. https://doi.org/10.1016/j.apsusc.2005.01.173
13. Zhang Y, Wang Y, Zhang J, Liu Y, Yang X, Zhang Q (2015) Micromachining features of TiC ceramic by femtosecond pulsed laser. Ceram Int 41:6525–6533. https://doi.org/10.1016/j.ceramint.2015.01.095
14. Chen B, Tsai Y, Ho C et al (2013) Parametric effects on femtosecond laser ablation of Al2O3 ceramics. Ceram Int 39:S341–S344. https://doi.org/10.1016/j.ceramint.2012.10.090
15. Li J, Ji L, Hu Y, Bao Y (2016) Precise micromachining of yttria-tetragonal zirconia polycrystal ceramic using 532 nm nanosecond laser. Ceram Int 42:4377–4385. https://doi.org/10.1016/j.ceramint.2015.11.118
16. Preusch F, Adelmann B, Hellmann R (2014) Micromachining of AlN and Al2O3 using fiber laser. micromachines 5:1051–1060. https://doi.org/10.3390/mi5041051
17. Liu Y, Liu L, Deng J, Meng R, Zou X, Wu F (2017) Fabrication of micro-scale textured grooves on green ZrO 2 ceramics by pulsed laser ablation. Ceram Int 43:6519–6531. https://doi.org/10.1016/j.ceramint.2017.02.074
18. Hanon MM, Akman E, Oztoprak BG et al (2012) Experimental and theoretical investigation of the drilling of alumina ceramic using Nd : YAG pulsed laser. Opt Laser Technol 44:913–922. https://doi.org/10.1016/j.optlastec.2011.11.010
19. Leone C, Genna S, Tagliaferri F, Palumbo B, Dix M (2016) Experimental investigation on laser milling of aluminium oxide using a 30 W Q-switched Yb : YAG fi ber laser. Opt Laser Technol 76:127–137. https://doi.org/10.1016/j.optlastec.2015.08.005
20. Bharatish A, Murthy HNN, Anand B et al (2013) Characterization of hole circularity and heat affected zone in pulsed CO 2 laser drilling of alumina ceramics. Opt Laser Technol 53:22–32. https://doi.org/10.1016/j.optlastec.2013.04.010
21. Kibria G, Doloi B, Bhattacharyya B (2013) Experimental investigation and multi-objective optimization of Nd : YAG laser micro-turning process of alumina ceramic using orthogonal array and grey relational analysis. Opt Laser Technol 48:16–27. https://doi.org/10.1016/j.optlastec.2012.09.036
22. Kibria G, Doloi B, Bhattacharyya B (2013) Predictive model and process parameters optimization of Nd : YAG laser micro-turning of ceramics. Int J Adv Manuf Technol 213–229. https://doi.org/10.1007/s00170-012-4161-9
23. Umer U, Khan M, Al-ahmari A (2017) Multi-response optimization of machining parameters in micro milling of alumina ceramics using Nd : YAG laser. Measurement 95:181–192. https://doi.org/10.1016/j.measurement.2016.10.004
24. Kuar AS, Acherjee B, Ganguly D, et al (2012) Optimization of Nd : YAG laser parameters for microdrilling of alumina with multiquality characteristics via Grey – Taguchi Method. Mater Manuf Process 27:329–336. https://doi.org/10.1080/10426914.2011.585493
25. Ganguly D, Acherjee B, Kuar AS, Mitra S (2012) Hole characteristics optimization in Nd : YAG laser micro-drilling of zirconium oxide by grey relation analysis. Int J Adv Manuf Technol 1255–1262. https://doi.org/10.1007/s00170-012-4090-7
26. Dhupal D, Doloi B, Bhattacharyya B (2008) Parametric analysis and optimization of Nd : YAG laser micro-grooving of aluminum titanate (Al 2 TiO 5). Ceramics:883–893. https://doi.org/10.1007/s00170-006-0913-8
27. Teixidor D, Ferrer I, Ciurana J, Özel T (2013) Optimization of process parameters for pulsed laser milling of micro-channels on AISI H13 tool steel. Robot Comput Integr Manuf 29:209–218. https://doi.org/10.1016/j.rcim.2012.05.005
28. Acherjee B, Prakash S, Kuar AS, Mitra S (2014) Grey relational analysis based optimization of underwater Nd : YAG laser micro-channeling on PMMA. Procedia Eng 97:1406–1415. https://doi.org/10.1016/j.proeng.2014.12.422
29. Ahmed N, Alahmari AM, Darwish S (2016) Laser beam micro-milling of nickel alloy : dimensional variations and RSM optimization of laser parameters. Appl Phys A Mater Sci Process 122:1–16. https://doi.org/10.1007/s00339-016-0553-2
30. Giorleo L, Ceretti E, Giardini C (2016) Optimization of laser micromachining process for biomedical device fabrication. Int J Adv Manuf Technol 82:901–907. https://doi.org/10.1007/s00170-015-7450-2
31. Gautam C, Joyner J, Gautam A, Rao J, Vajtai R (2016) Zirconia based dental ceramics: structure, mechanical properties, biocompatibility and applications. Dalt Trans 45:19194–19215. https://doi.org/10.1039/C6DT03484E
32. Whitesides GM (2006) The origins and the future of microfluidics. Nature 442:368–373. https://doi.org/10.1038/nature05058
33. Farhan Shafique M, Laister A, Clark M, Miles RE, Robertson ID (2011) Fabrication of embedded microfluidic channels in low temperature co-fired ceramic technology using laser machining and progressive lamination. J Eur Ceram Soc 31:2199–2204. https://doi.org/10.1016/j.jeurceramsoc.2011.05.039
34. Ong SE, Zhang S, Du HJ, Fu YQ (2008) Fundamental principles and applications of microfluidic systems. Front Biosci 13:2757–2773. https://doi.org/10.2741/2883
35. Becker H, Locascio LE (2002) Polymer microfluidic devices. Talanta 56:267–287. https://doi.org/10.1016/S0039-9140(01)00594-X
36. Abdo BMA, Anwar S, El-Tamimi AM et al (2018) Laser micro-milling of bio-lox forte ceramic: an experimental analysis. Precis Eng. https://doi.org/10.1016/j.precisioneng.2018.04.001
37. Guarino S, Ponticelli GS, Giannini O, et al (2017) Laser milling of yttria-stabilized zirconia by using a Q-switched Yb : YAG fiber laser : experimental analysis. https://doi.org/10.1007/s00170-017-1020-8
38. Montgomery DC (2013) Design and analysis of experiments. John Wiley & Sons, Inc
39. Teixidor D, Orozco F (2013) Effect of process parameters in nanosecond pulsed laser micromachining of PMMA-based microchannels at near-infrared and ultraviolet wavelengths. Int J Adv Manuf Technol 67:1651–1664. https://doi.org/10.1007/s00170-012-4598-x

40. Pham DTÃ, Dimov SS, Petkov PV (2007) Laser milling of ceramic components. Int J Mach Tools Manuf 47:618–626. https://doi.org/10.1016/j.ijmachtools.2006.05.002
41. Deville S, Chevalier J, Gremillard L (2006) Influence of surface finish and residual stresses on the ageing sensitivity of biomedical grade zirconia. Biomaterials 27:2186–2192. https://doi.org/10.1016/j.biomaterials.2005.11.021
42. Yin L, Nakanishi Y, Alao AR, Song XF, Abduo J, Zhang Y (2017) A review of engineered zirconia surfaces in biomedical applications. Procedia CIRP 65:284–290. https://doi.org/10.1016/j.procir.2017.04.057
43. modeFrontier | ESTECO. http://www.esteco.com/modefrontier. Accessed 28 Feb 2018